

# The Effect of Surface Charges on the Cellular Uptake of Liposomes Investigated by Live Cell Imaging

Ji Hee Kang<sup>1</sup> · Woo Young Jang<sup>1</sup> · Young Tag Ko<sup>1</sup>

Received: 25 August 2016 / Accepted: 4 January 2017 / Published online: 11 January 2017  
© Springer Science+Business Media New York 2017

## ABSTRACT

**Purpose** Liposomes have been developed as versatile nanocarriers for various pharmacological agents. The effect of surface charges on the cellular uptake of the liposomes has been studied by various methods using mainly fixed cells with inevitable limitations. Live cell imaging has been proposed as an alternative methods to overcome the limitations of the fixed cell-based analysis. In this study, we aimed to investigate the effects of surface charges on cellular association and internalization of the liposomes using live cell imaging.

**Methods** We studied the cellular association and internalization of liposomes with different surface charge using laser scanning confocal microscopy (LSCM) equipped with live cell chamber system. Flow cytometry was also carried out using flow cytometer (FACS) for comparison.

**Results** All of the cationic, neutral and anionic liposomes showed time-dependent cellular uptake through specific endocytic pathways. In glioblastoma U87MG cells, the cationic and anionic liposomes were mainly taken up *via* macropinocytosis, while the neutral liposomes mainly *via* caveolae-mediated endocytosis. In fibroblast NIH/3T3 cells, all of the three liposomes entered into the cell *via* clathrin-mediated endocytosis.

**Conclusions** This study provides a better understanding on the cellular uptake mechanisms of the liposomes, which could contribute significantly to development of liposome-based drug delivery systems.

**KEY WORDS** cellular uptake · confocal microscopy · endocytosis · flow cytometer · liposomes

## ABBREVIATIONS

CD	Cytochalasin D
CPZ	Chlorpromazine
DIC	Differential interference contrast
DLS	Dynamic light scattering
DMEM	Dulbecco's modified eagle's medium
FACS	Flow cytometer
GS	Genistein
HBG	HEPES buffered glucose (10 mM HEPES, 5% glucose, pH 7.4)
HBS	HEPES buffered saline (10 mM HEPES, 150 mM NaCl, pH 7.4)
LSCM	Laser scanning confocal microscopy
PBS	Phosphate buffered saline
PDI	Polydispersity index
PEG-	1,2-Distearoyl- <i>sn</i> -Glycero-3-
PE	Phosphoethanolamine-N-[Methoxy (Polyethylene glycol)-2000]
POPC	1-Palmitoyl-2-Oleoyl- <i>sn</i> -Glycero-3-Phosphocholine
POPG	1-Palmitoyl-2-Oleoyl- <i>sn</i> -Glycero-3-[Phospho-rac-91-glycerol]
PTRF	Polymerase I and transcript release factor
Rh-PE	1,2-dioleoyl- <i>sn</i> -glycero-3-phosphoethanolamine-N-(lissamine rhodamine B sulfonyl)

Ji Hee Kang and Woo Young Jang contributed equally to this work.

**Electronic supplementary material** The online version of this article (doi:10.1007/s11095-017-2097-3) contains supplementary material, which is available to authorized users.

✉ Young Tag Ko  
youngtakko@gachon.ac.kr

<sup>1</sup> College of Pharmacy and Gachon Institute of Pharmaceutical Sciences, Gachon University, 191 Hambakmoe-ro, Yeonsu-gu, Incheon, South Korea 21936

## INTRODUCTION

Liposomes have been developed as versatile nanocarriers for various pharmacological agents, and thus applied for marketed formulations such as Doxil and Ambisome (1). Liposomes have a lot of advantages such as biocompatibility, biodegradability, low-toxicity, long half-life, and high cargo loading capacity (2,3). Liposomes also can be engineered for specific applications by grafting certain functionality onto the surfaces, *i.e.*, PEGylation for long circulation or specific ligand attachment for targeting. Besides, surface charge has been implicated for non-specific interactions with blood components during circulation and cell membranes within tissues. The non-specific interactions with cell membranes triggered by surface charges could affect the subsequent intracellular internalization of the liposomes (4), which could occur *via* different endocytic pathways (5,6), *i.e.*, clathrin-mediated endocytosis, caveolae-mediated endocytosis and macropinocytosis (7) and destined to lysosomes for degradation.

The effect of surface charge on the cellular uptake has been studied by various methods including microscopic or flow cytometric analysis (4,8). However, those methods have been applied mainly to fixed cells not to live cells. Fixed cell-based analysis is subjected to inevitable limitations. Live cell imaging has been proposed as an alternative methods to overcome the limitations of fixed cell-based analysis (9). Live cell imaging on individual cells allows following dynamic cellular processes that is difficult in fixed cell. Time-lapse imaging on the live cells could be an effective tool to observe various cellular function dynamics such as cell division, cell proliferation and organelle or chromosome dynamics (10), leading to optimization and characterization at the single cell level and thus providing significant contributions to drug discovery (11). In particular, confocal time-lapse imaging on the live cells has been applied in many studies for drug discovery such as intracellular dynamics, transgene expression and behavior of particles in cells (12–14).

It was reported that cancer cells have many different characteristics, including loss of differentiation, increased invasiveness, and decreased drug sensitivity, compared with normal cells (15). And, the cancer cells have the extracellular environment with acidic pH and more alkaline intracellular environment when compared to normal cells (16). In addition, difference in membrane potentials was observed between cancer cells and normal cells (17) and it would lead to difference in cellular interaction and internalization of the liposomes.

In this study, we aimed to investigate the effects of surface charges on cellular association and internalization of the liposomes using live cell imaging technique with LSCM with live cell chamber. Flow cytometry was also carried out for comparison. Liposomes with different surface charges, *i.e.*, cationic, neutral and anionic, were prepared with fluorescent labeling and real-time images upon cellular exposure were

recorded in cancer and normal cells. Human glioblastoma U87MG and mouse fibroblast NIH/3T3 were used as a representative of cancer and normal cells, respectively.

## MATERIALS AND METHODS

### Materials

1-Palmitoyl-2-Oleoyl-*sn*-Glycero-3-Phosphocholine (POPC), 1-Palmitoyl-2-Oleoyl-*sn*-Glycero-3-[Phospho-rac-91-glycerol] (POPG), 1,2-Distearoyl-*sn*-Glycero-3-Phosphoethanolamine-N-[Methoxy(Polyethylene glycol)-2000] (PEG-PE), 1,2-dioleoyl-*sn*-glycero-3-phosphoethanolamine-N-(lissamine rhodamine B sulfonyl) (Rh-PE) cholesterol were purchased from Avanti Polar Lipids (Alabaster, AL). The 35 mm glass bottom cell culture dishes were purchased from SPL LifeSciences Co., LTD (Gyeonggi-do, South Korea). LysoTracker Deep Red and Hoechst 33342 were purchased from Thermo Fisher Scientific (Waltham, MA). Endocytosis inhibitors including chlorpromazine hydrochloride and genistein were purchased from Tokyo Chemical Industry (Tokyo, Japan). Cytochalasin D was purchased from Sigma-Aldrich (St Louis, MO). All other reagents were reagent grade.

### Preparation and Characterization of Liposomes

Three types of liposomes were prepared as previously described (18,19). Briefly, the following amounts of lipid were dissolved in chloroform: POPC (6.0  $\mu\text{mol}$ ), cholesterol (3.0  $\mu\text{mol}$ ), PEG-PE (0.3  $\mu\text{mol}$ ), Rh-PE (0.02  $\mu\text{mol}$ ), and either DOTAP (1.0  $\mu\text{mol}$ ) or POPC (1.0  $\mu\text{mol}$ ) or POPG (1.0  $\mu\text{mol}$ ) for cationic, neutral and anionic liposomes, respectively. Chloroform was removed by vacuum evaporation using a rotary evaporator (500 mmHg, 4 h, 30°C). The dried lipid film was hydrated with HBG buffer (10 mM HEPES, 5% glucose, pH 7.4) and incubated at room temperature for 4 h with intermittent mixing. The resulting suspension was extruded 11 times through a stack of two polycarbonate membranes of 100 nm pore size by employing a hand-held extruder (Avestin, Ottawa, Canada).

For measurement of size distribution and zeta potential, each sample was diluted with HBS (10 mM HEPES, 150 mM NaCl, pH 7.4) to obtain an optimal scanning intensity. Hydrodynamic diameter, polydispersity index (PDI) and zeta potential were measured 5 times by dynamic light scattering (DLS) using a zeta-potential and particle size analyzer (ELSZ-1000, Otsuka Electronics Co, Osaka, Japan). Scattered light was detected at 23°C at an angle of 90°. A viscosity value of 0.933 mPa and a refractive index of 1.333 were used for the data analysis. The instrument was routinely calibrated using a latex microsphere suspension.

### *In Vitro* Cellular Uptake by LSCM Live Cell Imaging

The human glioblastoma U87MG cells (passage 7) and mouse embryonic fibroblast NIH/3T3 cells (passage 7) were grown in DMEM medium supplemented with 10% fetal bovine serum (FBS) and 1% penicillin/streptomycin (complement medium) in a glass bottom cell culture dishes (35 mm, SPL) at a concentration of  $2 \times 10^3$  cells per well. The cells were stained by LysoTracker Deep Red (50  $\mu\text{g}/\text{ml}$ ) (Life Technologies) at 37°C for 90 min and Hoechst 33342 (1 mg/ml) (Life Technologies) at 37°C for 20 min. Subsequently, a single cell with clear morphology was chosen through observation in differential interference contrast (DIC) channel. The cells were treated with the liposomes labeled with Rh-PE at a total lipid concentration of 10  $\mu\text{g}/\text{ml}$  and then immediately observed using a laser scanning confocal microscope (LSCM, Al Plus, Nikon) with 60X oil immersion objective (numerical aperture 1.2) and live cell chamber system. Confocal z section images of 0.8  $\mu\text{m}$  thickness containing the maximal intensity of lysosomes were acquired every 3 min over 30 min periods and analyzed for Pearson's correlation using a image analysis software (NIS-E, Nikon).

### Investigation of Endocytic Pathways by LSCM Live Cell Imaging

To further investigate the uptake pathways, the cells (passage 8 or 9) were prepared as above. Before treatment with the liposomes, the cells had been pre-incubated with different inhibitors; chlorpromazine (10  $\mu\text{g}/\text{mL}$ ) to inhibit the formation of clathrin vesicles, genistein (54  $\mu\text{g}/\text{mL}$ ) to inhibit the formation of caveolae vesicles and cytochalasin D (10  $\mu\text{g}/\text{mL}$ ) to inhibit macropinocytosis at 37°C for 1 h. The media containing the inhibitors were replaced with the serum free media containing the liposomes at a total lipid concentration of 10  $\mu\text{g}/\text{mL}$ . The cells were analyzed for 30 min as above.

## RESULTS

### Preparation and Characterization of Liposomes

The liposomes were prepared according to a well-established procedure of dehydration-rehydration-membrane extrusion.

It was previously reported that 10 mol % of DOTAP along with 3 mol % of PEG successfully led to cationic or anionic liposomes with higher surface charges (20). For both of the lipid compositions, the procedure led to transparent and stable suspensions with narrow and uniform size distributions of average diameter of around 110 nm and zeta potential greater than  $\pm 10$  mV (Table I).

### *In Vitro* Cellular Uptake by LSCM Live Cell Imaging

The cationic liposomes readily entered into the live U87MG cells (Fig. 1a). The distinct and particulate red fluorescence were readily detected in the cell membranes and lysosomal compartments as early as 7 min and continued to accumulate into the lysosomal compartments along with relatively weak diffusion into the cytoplasm. However, there were no signs of nuclear co-localization with the cationic liposomes over 30 min periods. In contrast, no significant accumulation into the lysosomal compartments was observed for both the neutral and anionic liposomes (Fig. 1b and c). Image analysis for Pearson's correlation coefficient ( $r$ ), which could vary from +1 in the case of a perfect positive linear correlation to -1 in the case of a perfect negative linear anti-correlation, with zero if uncorrelated (21,22), further revealed the preferential accumulation of the cationic liposomes into lysosomal compartments over neutral and anionic liposomes. The  $r$  value of the cationic liposomes reached 0.8 at 3 min and then remained around 0.8 over 30 min periods, while the  $r$  value of the neutral liposomes was only 0.4 at 3 min and then slowly increased up to 0.6 over 30 min periods. No significant difference in lysosomal accumulation was observed between the anionic and neutral liposomes. Nuclear accumulation was not significant for all the liposomes (Fig. 1d and e). The cellular uptake of the three liposomes in NIH/3T3 cells was similar to that in U87MG cells (Fig. 2). Surprisingly, the cationic liposomes started to appear in the cell membranes and lysosomal compartments as early as 1 min and continued to accumulate into the lysosomal compartments.

In an attempt to further verify the above observations, the cellular uptake of the liposomes was also measured over a population of U87MG and NIH/3T3 cells using flow cytometer (FACS). The method and results of flow cytometry

**Table I** Size Distribution, PDI and Zeta Potential (Mean  $\pm$  s.e.m,  $n = 5$ )

	Cationic Liposomes	Neutral Liposomes	Anionic Liposomes
Diameter (nm)	111.3 $\pm$ 2.4	112.8 $\pm$ 1.8	119.3 $\pm$ 2.7
PDI	0.6 $\pm$ 0.02	0.54 $\pm$ 0.01	0.53 $\pm$ 0.02
Zeta potential (mV)	43.2 $\pm$ 0.1	-5.1 $\pm$ 0.2	-15.85 $\pm$ 0.8

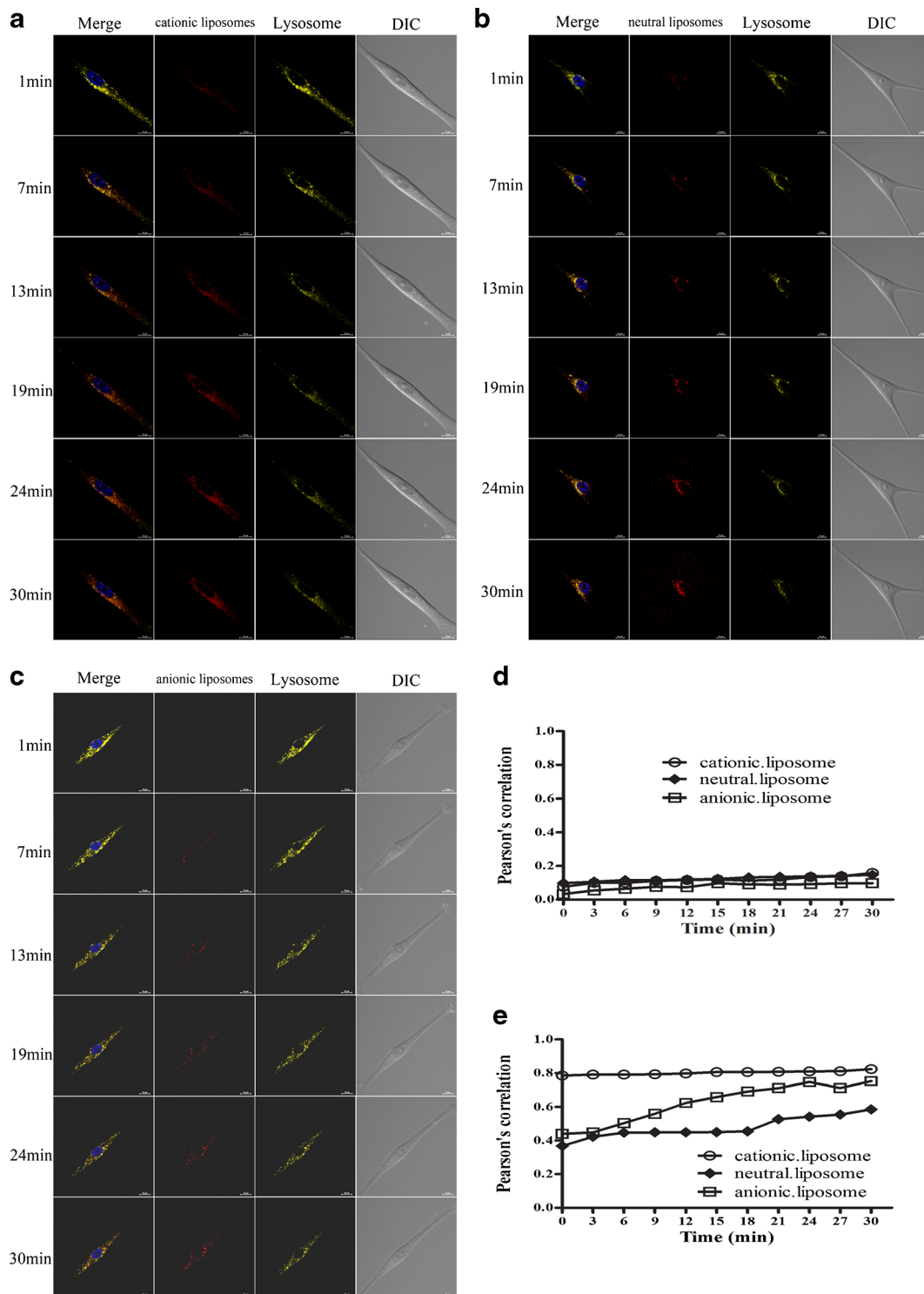


**Fig. 1** The cellular uptake of **(a)** cationic liposomes **(b)** neutral liposomes **(c)** anionic liposomes in U87MG cells using LSCM over 30 min. Co-localization of the liposomes with cellular **(d)** nucleus and **(e)** lysosome. Co-localization is demonstrated within the merged images and quantified using Pearson's correlation. Pearson's correlation for co-localization of fluorescent signals was determined for indicated images. Blue channel (Hoechst 33342): nucleus; yellow channel (LysoTracker Deep Red): lysosome; red channel: Rh-PE-labeled liposomes with different surface charges.

were described in [Supplementary material](#). As shown in [Fig. S1](#), when incubated with the liposomes for 30 min

periods, the cationic liposomes were taken up greater than the neutral and anionic liposomes in both U87MG and

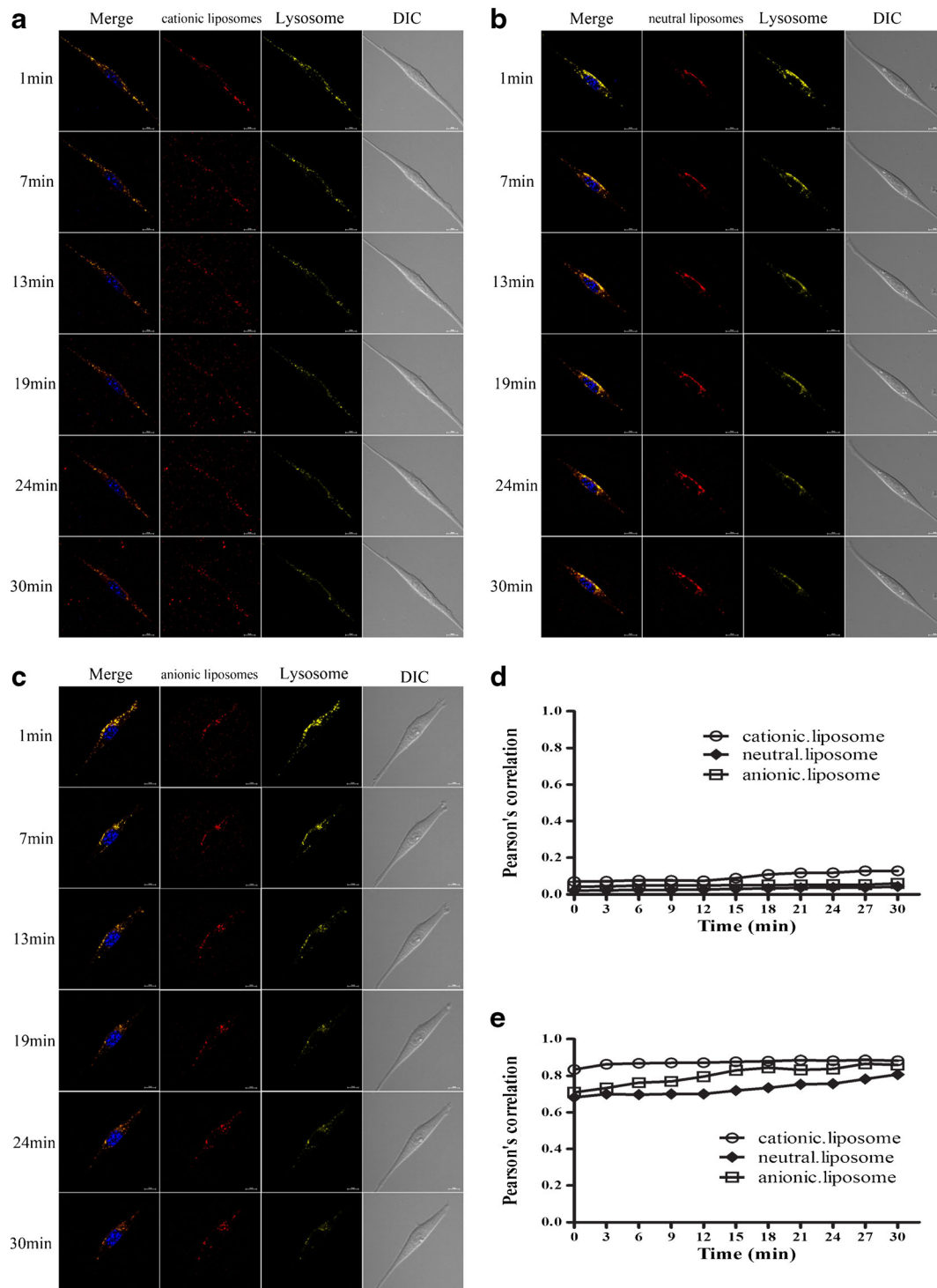


**Fig. 2** The cellular uptake of **(a)** cationic liposomes **(b)** neutral liposomes **(c)** anionic liposomes in NIH/3T3 cells by LSCM live cell imaging. Co-localization of the liposomes with cellular **(d)** nucleus and **(e)** lysosome. Blue channel (Hoechst 33342); nucleus; yellow channel (LysoTracker Deep Red); lysosome; red channel: Rh-PE-labeled liposomes with different surface charges.

NIH/3T3 cells, which is well consistent with the results from LSCM live cell imaging.

All together, the lysosomal accumulation *via* endocytosis was profound in the cationic liposomes as compared to the neutral and anionic liposomes.

### Investigation of Endocytic Pathways in U87MG Cells by LSCM Live Cell Imaging

To further investigate the cellular uptake mechanisms of the liposomes, U87MG and NIH/3T3 cells were treated

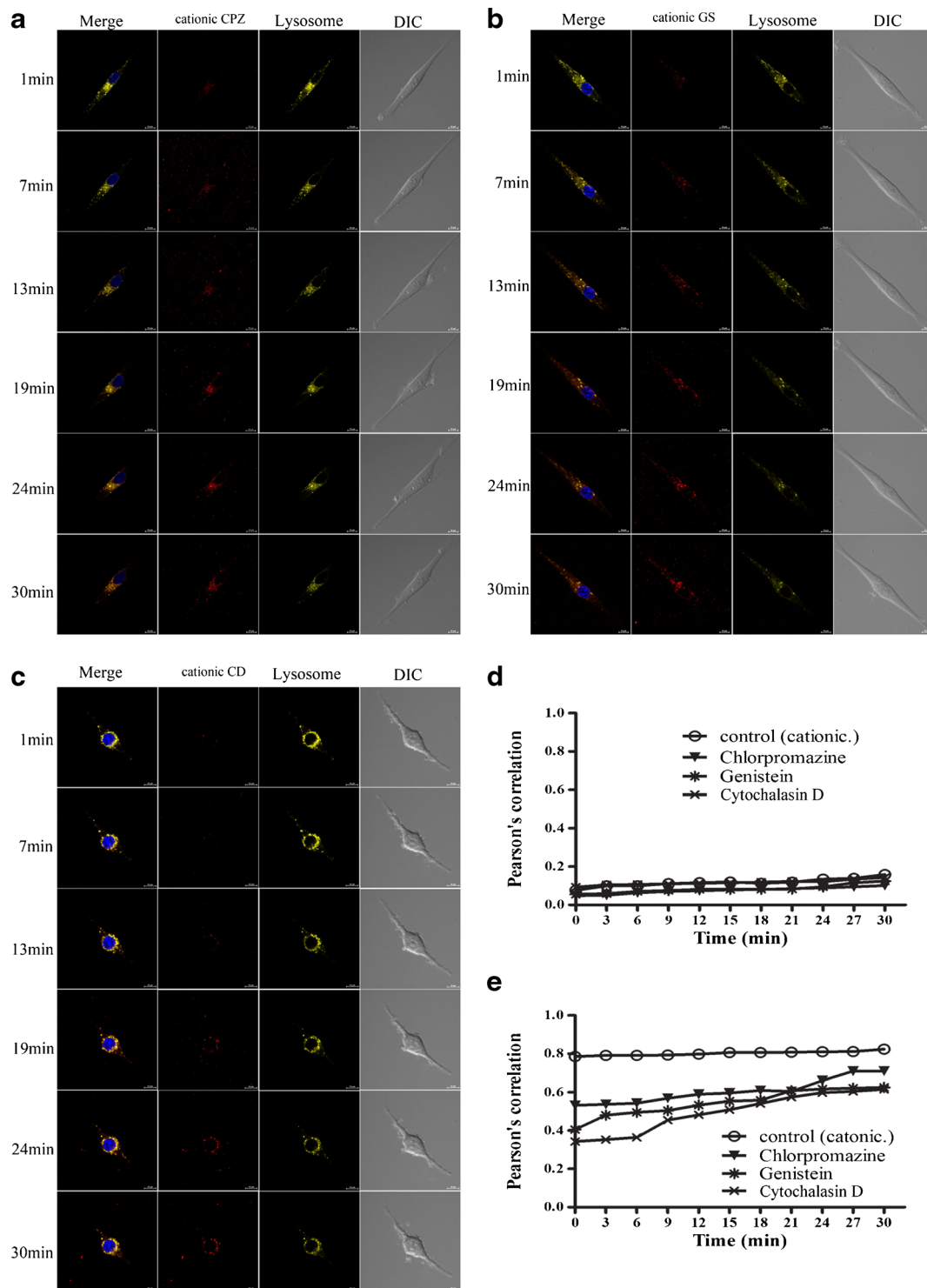


**Fig. 3** Endocytic pathways of the cationic liposomes in U87MG cells. The confocal microscopy images of U87MG cells pre-incubated with chlorpromazine (**a**), genistein (**b**), or cytochalasin D (**c**) for 1 h at 37°C. Co-localization of the liposomes with cellular nucleus (**d**) and lysosome (**e**). Blue channel (Hoechst 33342): nucleus; yellow channel (LysoTracker): lysosome; red channel (Rh-PE-labeled liposomes).

with chlorpromazine (CPZ), genistein (GS) and cytochalasin D (CD) that inhibit clathrin-mediated endocytosis, caveolae-mediated endocytosis and macropinocytosis, respectively. In U87MG cells, the cationic liposomes

appeared in lysosomal compartments at 13 min after blocking the clathrin-mediated endocytosis (CPZ) and caveolae-mediated endocytosis (CD) (Fig. 3a and b), while only at 19 min after blocking the macropinocytosis (GS)

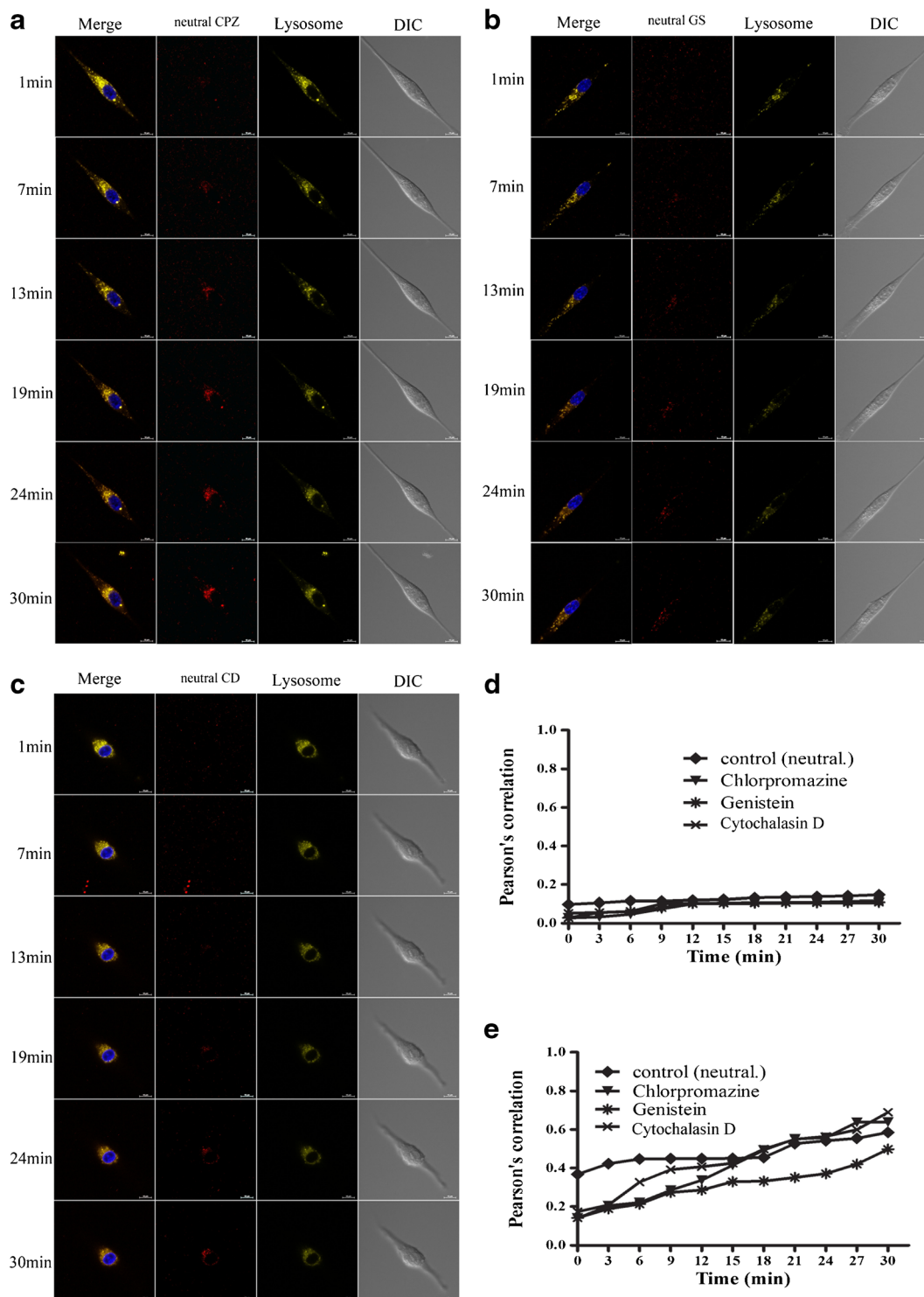


**Fig. 4** Endocytic pathways of the neutral liposomes in U87MG cells. The confocal microscopy images of U87MG cells pre-incubated with chlorpromazine (**a**), genistein (**b**), or cytochalasin D (**c**) for 1 h at 37°C. Co-localization of the liposomes with cellular nucleus (**d**) and lysosome (**e**). Blue channel (Hoechst 33342): nucleus; yellow channel (LysoTracker): lysosome; red channel: Rh-PE-labeled liposomes.

(Fig. 3c). Upon inhibition, Pearson's correlation coefficient  $r$  values between the cationic liposomes and lysosomal compartments were from 0.35 only up to 0.7, which were significantly low compared to those without inhibition. In

particular, the  $r$  values upon blocking macropinocytosis showed dramatic decrease from 0.8 to 0.35. No significant difference was observed in nuclear accumulation upon inhibition of the uptake pathways (Fig. 3d and e).

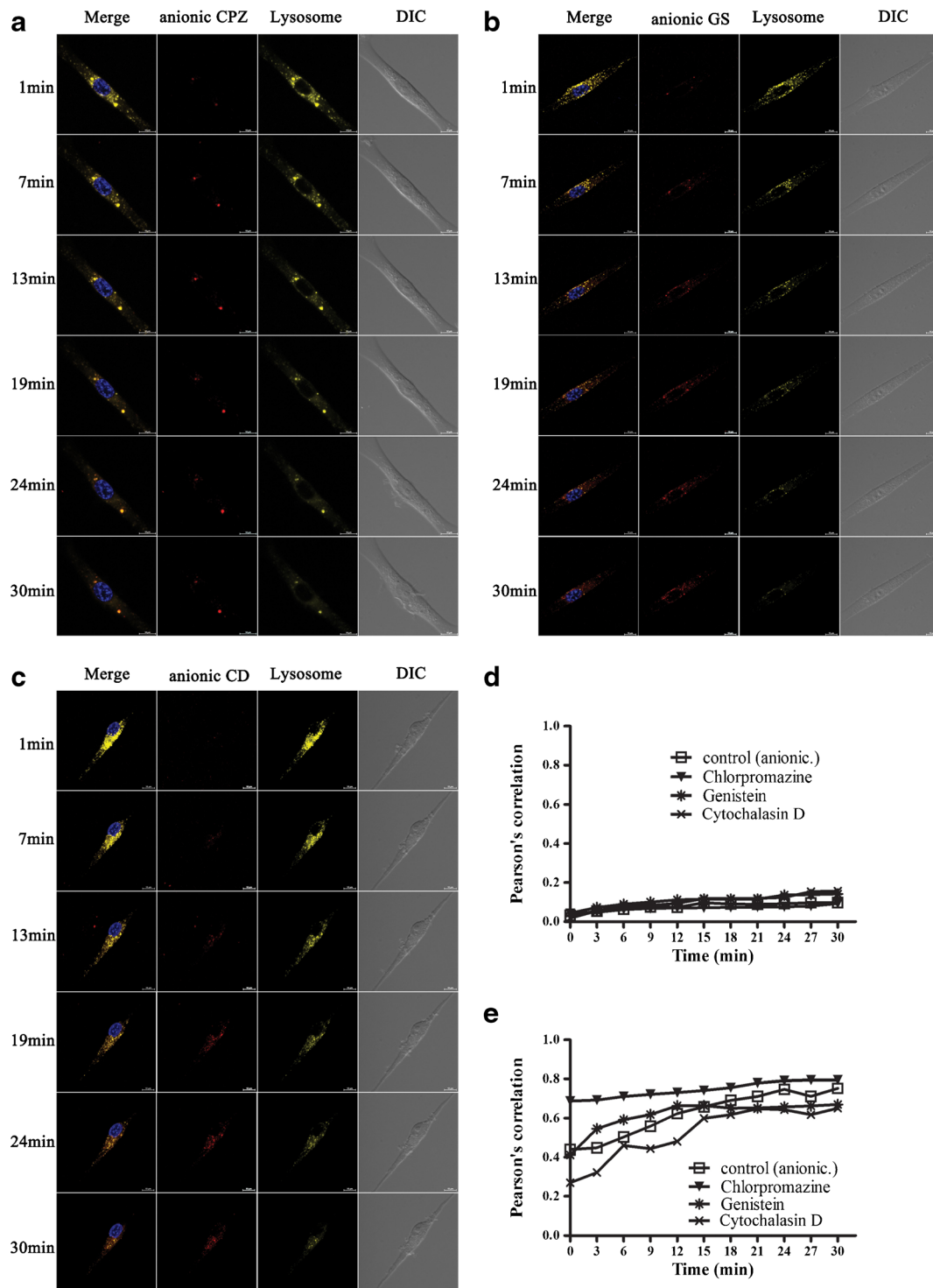


**Fig. 5** Endocytic pathways of the anionic liposomes in U87MG cells. The confocal microscopy images of U87MG cells pre-incubated with chlorpromazine (**a**), genistein (**b**), or cytochalasin D (**c**) for 1 h at 37°C. Co-localization of the liposomes with cellular nucleus (**d**) and lysosome (**e**). Blue channel (Hoechst 33342): nucleus; yellow channel (LysoTracker): lysosome; red channel: Rh-PE-labeled liposomes.

The neutral liposomes started to accumulate in lysosomal compartments at 13, 19 and 24 min in U87MG cells pre-treated with CPZ, GS and CD, respectively (Fig. 4a–c). In contrast to the cationic liposomes, the neutral liposomes showed no considerable differences in lysosomal accumulations

upon inhibition of the endocytic pathways, leading to almost identical  $r$  values after 15 min upon CPZ or CD treatment. Similarly to the cationic liposomes, no significant difference was observed in nuclear accumulation upon inhibition of the uptake pathways (Fig. 4d and e).



**Table II** The Relative Potency of Endocytosis of the Liposomes in U87MG Cells

The relative potency of endocytosis in U87MG					
Cationic liposomes	Macropinocytosis	>	Caveolae mediated endocytosis	>	Clathrin-mediated endocytosis
Neutral liposomes	Caveolae mediated endocytosis	>	Macropinocytosis	>	Clathrin-mediated endocytosis
Anionic liposomes	Macropinocytosis	>	Caveolae mediated endocytosis	>	Clathrin-mediated endocytosis

The anionic liposomes started to accumulate in lysosomal compartments at 7 min upon inhibition of clathrin-mediated (CPZ) and caveolae-mediated (CD) endocytosis and then the liposomes were diffused into the cytoplasm (Fig. 5a and b) while only at 19 min upon inhibition of macropinocytosis (GS) (Fig. 5c). Similar with the cationic liposomes, the r value showed significant decreases from 0.7 to 0.3 upon inhibition of the macropinocytosis pathways (GS). No significant difference was observed in nuclear accumulation upon inhibition of the uptake pathways (Fig. 5d and e).

In an attempt to further verify the above observations, the cellular uptake of the liposomes upon inhibition was also measured over a population of U87MG cells using flow cytometer (FACS) (Fig. S2). When incubated with the liposomes for 30 min periods upon inhibition, the main endocytic pathway of the liposomes in U87MG cells were determined to be well consistent with the results from LSCM live cell imaging.

All together, the relative potency of the uptake pathways in U87MG cells for the liposomes was summarized in Table II.

### Investigation on Endocytic Pathways in NIH/3T3 Cells by LSCM Live Cell Imaging

In order to further investigate the endocytic pathway of the liposomes in normal cells, NIH/3T3 cells were treated with inhibitors and observed as above. Upon pre-treatment with CPZ or CD, the cationic liposomes began to appear in periphery of the cells at 7 min, and then in lysosomal compartments at 13 min (Fig. 6a and c). Upon inhibition of the caveolae-mediated endocytosis (GS), the cationic liposomes began to appear in the lysosomal compartments as early as 1 min and continued to accumulate into the lysosomal compartments (Fig. 6b). Upon inhibition, the r values between the cationic liposomes and lysosomal compartments were from 0.2 only up to 0.7, which were significantly low compared to those without inhibition. No significant difference was observed in nuclear accumulation upon inhibition of the uptake pathways (Fig. 6d and e).

Both the neutral and anionic liposomes started to be detected in lysosomal compartments at 13 min after blocking clathrin-mediated endocytosis (CPZ) and macropinocytosis (CD), while at 7 min after blocking caveolae-mediated endocytosis (GS) (Figs. 7a–c and 8a–c). Upon inhibition, the r values between the neutral liposomes and lysosomal

compartments were from 0.3 only up to 0.6, which were significantly low compared to those without inhibition, leading to the dramatic decrease from 0.7 to 0.3 upon treatment with CPZ. No significant difference was observed in nuclear accumulation upon inhibition of the uptake pathways (Figs. 7d and 8d). This indicated that the cellular uptake of the neutral liposomes was mainly mediated *via* clathrin-mediated endocytosis (Figs. 7e and 8e).

In an attempt to further verify the above observations, the cellular uptake of the liposomes upon inhibition was also measured over a population of NIH/3T3 cells using flow cytometer (FACS) (Fig. S3). When incubated with the liposomes for 30 min periods upon inhibition, the main endocytic pathway of the liposomes in NIH/3T3 cells were determined to be well consistent with the results from LSCM live cell imaging.

All together, the relative potency of the uptake pathways in NIH/3T3 cells for the liposomes was summarized in Table III.

## DISCUSSION

Liposomes have been utilized as promising drug delivery carriers for efficient cancer treatment (23). We already studied about liposomes encapsulated various bioactive molecules such as nucleic acids (18,19), nanoparticles (20,24) and small molecules (25). Physicochemical characteristics of the liposomes such as size, surface charge, hydrophobicity, drug loading and encapsulating efficiency have been proposed to be crucial for the development of suitable liposomes for drug delivery (26–28). In particular, the surface charges have shown critical effects on the *in vitro* and *in vivo* behavior of liposomes. In this report, we investigated the cellular uptake of the liposomes focused on the difference of surface charge.

All of the cationic, neutral and anionic liposomes showed time-dependent uptake *via* endocytosis and lysosomal accumulation, which were the most profound in the cationic liposomes with no significant difference between the neutral and anionic liposomes. While positively charged lipids in the cationic liposomes could be attracted to the negatively charged cell membrane by electrostatic interaction, the neutral and anionic liposomes do not have such electrostatic interaction with the cell membrane, leading to decreased

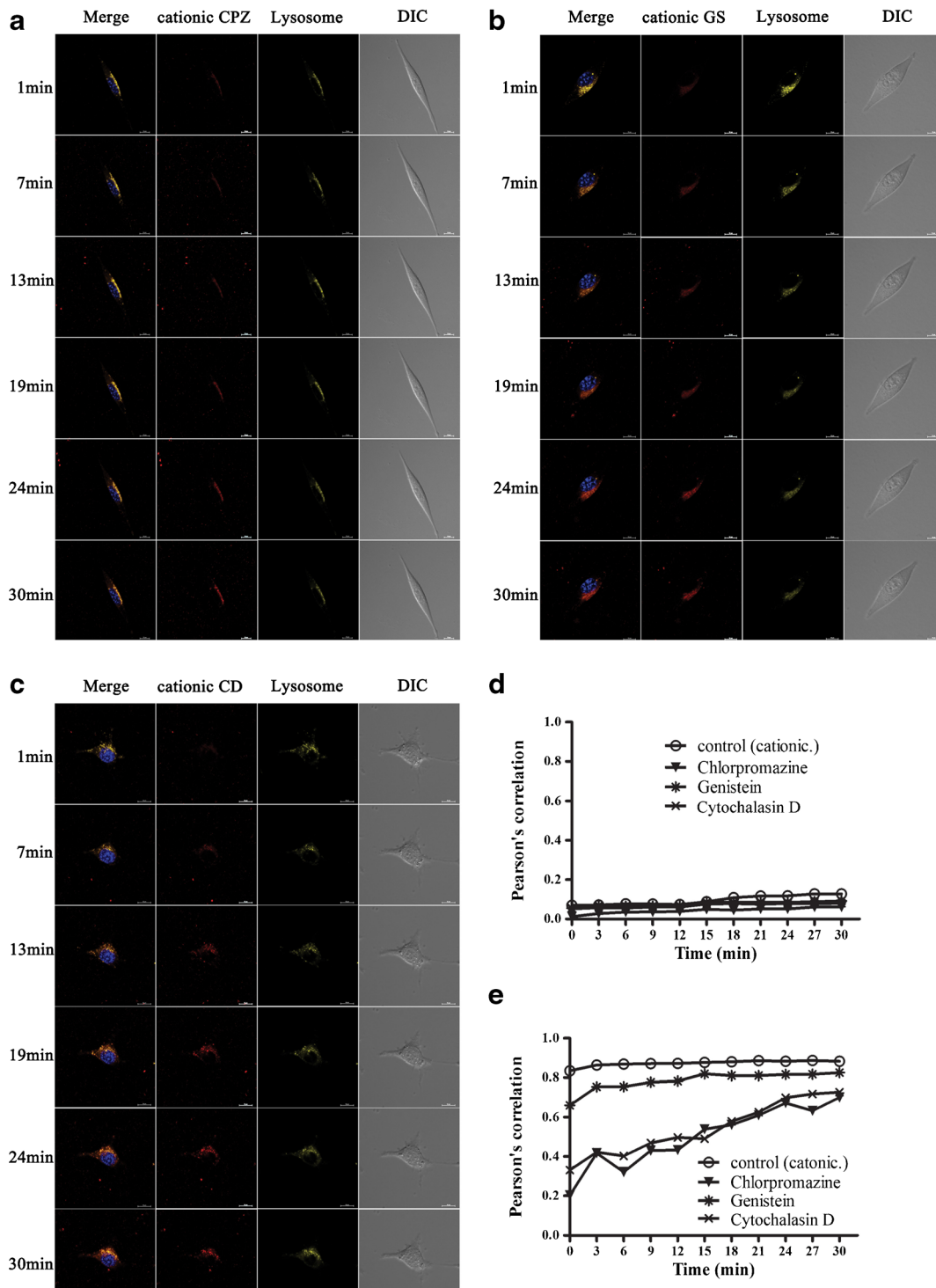


**Fig. 6** Endocytic pathways of the cationic liposomes in NIH/3T3 cells. The confocal microscopy images of NIH/3T3 cells pre-incubated with chlorpromazine (**a**), genistein (**b**), or cytochalasin D (**c**) for 1 h at 37°C. Co-localization of the liposomes with cellular nucleus (**d**) and lysosome (**e**). Blue channel (Hoechst 33342): nucleus; yellow channel (LysoTracker): lysosome; red channel: Rh-PE-labeled liposomes.

cellular uptake compared to the cationic liposomes (29). It was also reported that absorption of anionic liposomes into the cells was hindered due to electrical repulsion from cell membrane surface (30).

The cellular uptake of the cationic liposomes was four-fold higher in U87MG cells than NIH/3T3 cells (Fig. S1). It was reported that cancer cells have more acidic environment and higher membrane potentials than normal cells, which could

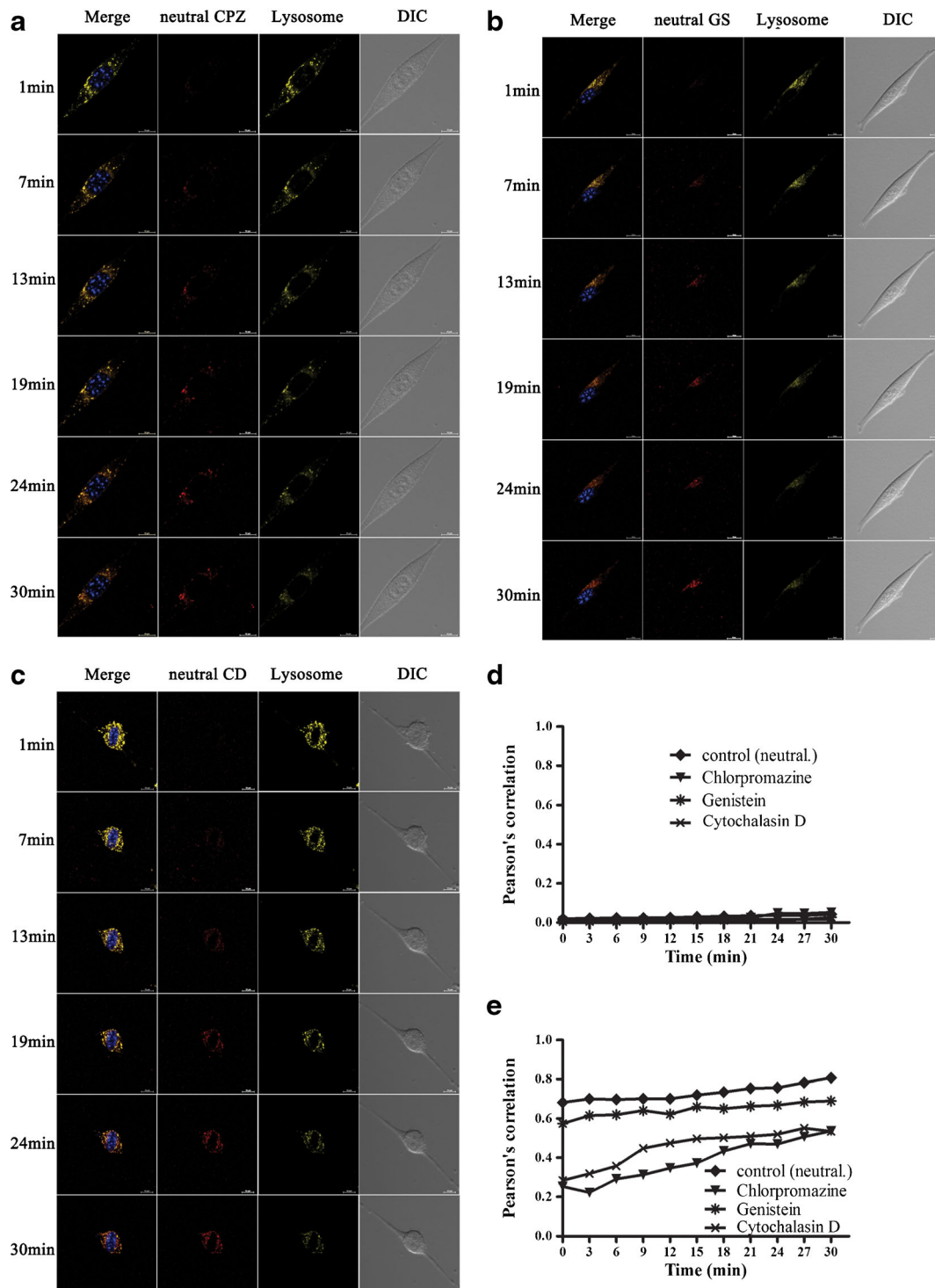


**Fig. 7** Endocytic pathways of the neutral liposomes in NIH/3T3 cells. The confocal microscopy images of NIH/3T3 cells pre-incubated with chlorpromazine (**a**), genistein (**b**), or cytochalasin D (**c**) for 1 h at 37°C. Co-localization of liposome with cellular nucleus (**d**) and lysosome (**e**). Blue channel (Hoechst 33342): nucleus; yellow channel (LysoTracker): lysosome; red channel: Rh-PE-labeled liposomes.

lead to more interaction with the cationic lipids in the cationic liposomes. The cationic lipid DOTAP in the cationic liposomes can be protonated in acidic conditions (31), it would lead to high cellular uptake into cancer cells which have a relatively low pH environment compared to normal cells (32,33).

The main endocytic pathways of the liposomes were also investigated using LSCM live cell imaging after treatment with various inhibitors and then compared to FACS analysis. The inhibitors used in this study have been widely used for investigation of endocytosis mechanisms (34,35) and

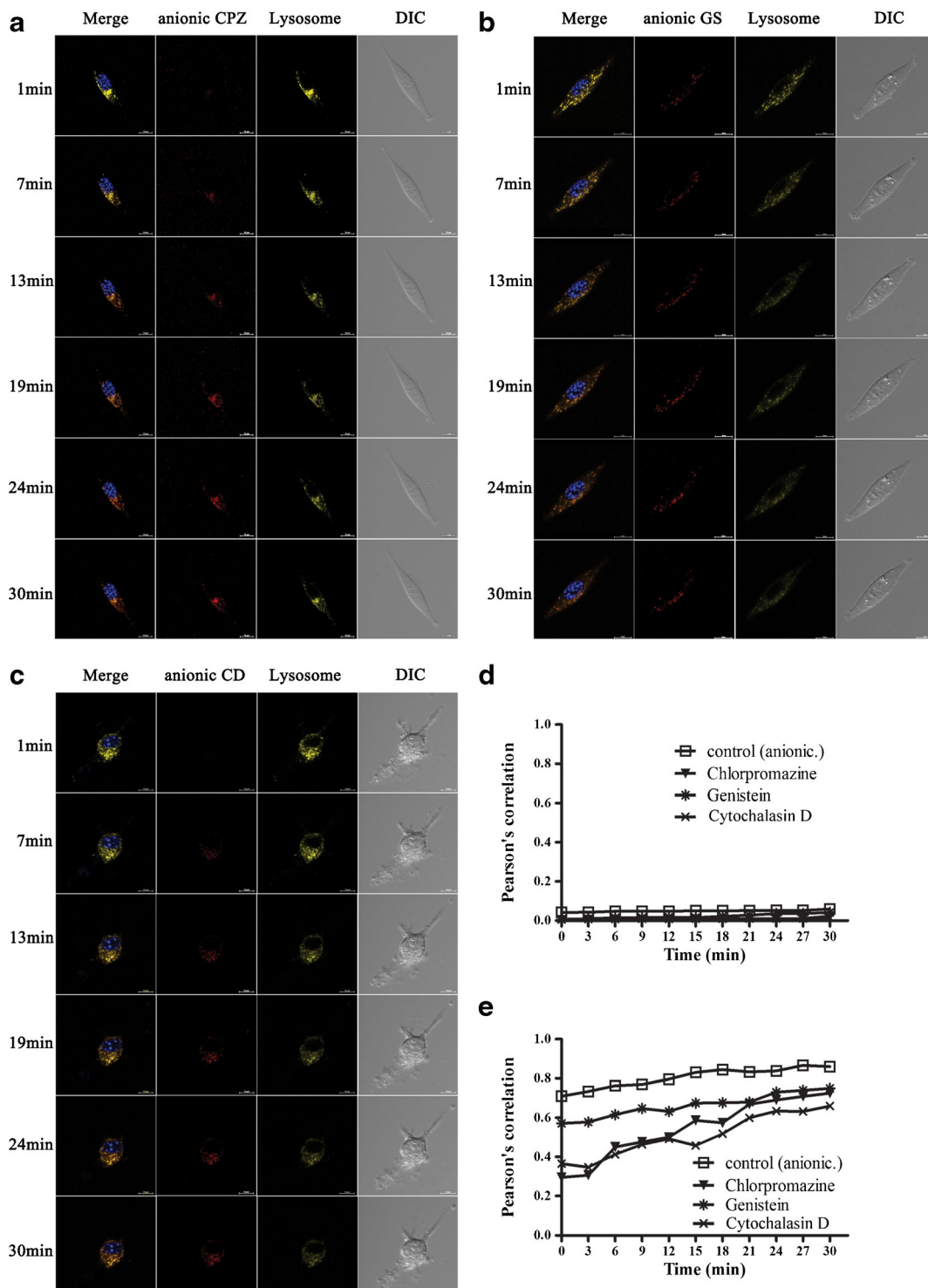


**Fig. 8** Endocytic pathways of the anionic liposomes in NIH/3T3 cells. The confocal microscopy images of NIH/3T3 cells pre-incubated with chlorpromazine (**a**), genistein (**b**), or cytochalasin D (**c**) for 1 h at 37°C. Co-localization of the liposomes with cellular nucleus (**d**) and lysosome (**e**). Blue channel (Hoechst 33342): nucleus; yellow channel (LysoTracker): lysosome; red channel: Rh-PE-labeled liposomes.

the mechanism and limitation of these inhibitors have been studied in reviews (36–38). After blocking the endocytic pathways, the liposomes were slowly accumulated in the lysosomal compartments as compared to the control in both U87MG and NIH/3T3 cells (Figs. 4, 5, 6, 7 and 8). The main endocytic

pathways from LSCM live cell imaging were consistent with those from FACS, although a minor difference was observed in the relative potency between LSCM and FACS. The minor difference might be due to the difference in cell number employed in analysis. A single cell was monitored over time

**Table III** The Relative Potency of Endocytosis of the Liposomes in NIH/3T3 Cells

The relative potency of endocytosis in NIH/3T3					
Cationic liposomes	Clathrin-mediated endocytosis	>	Macropinocytosis	>	Caveolae mediated endocytosis
Neutral liposomes	Clathrin-mediated endocytosis	>	Macropinocytosis	>	Caveolae mediated endocytosis
Anionic liposomes	Clathrin-mediated endocytosis	>	Macropinocytosis	>	Caveolae mediated endocytosis

in LSCM live cell imaging, whereas a population of cells with 30,000 counts was monitored in FACS.

In U87MG cells, the main endocytic pathways of the cationic liposomes were macropinocytosis, by which extracellular substances were taken up into the cells in the way of macropinosomes (0.2–5  $\mu\text{m}$  in diameter) (39). Although the average size of the cationic liposomes is  $111.3 \pm 2.4$  nm, they might quickly attach to the cell surface close to each other, forming bigger aggregates, and enter together into the cells as macropinosomes. Caveolae-mediated endocytosis involves the process of the cellular entry by the formation of caveolae vesicles on the cell membranes abundant cholesterol and glycosphingolipids (40,41). It could be speculated that caveolae-mediated endocytosis be the main uptake pathways for the neutral liposomes due to the cholesterol provided from the neutral liposomes.

In NIH/3T3 cells, the cellular uptake of the cationic, neutral and anionic liposomes was more affected by clathrin-mediated than macropinocytosis or caveolae-mediated endocytosis. In clathrin-mediated endocytosis, specific ligands such as cholesterol bind to receptors on the cell membrane, then clathrin-coated pits were formed with 100–150 nm diameters and entered into the cells (42,43). The effect of surface charges on the interaction between the liposomes and NIH 3T3 cell might play a less critical role whereas specific binding between molecular components in the liposomes and cell membranes plays a more critical role (42).

## CONCLUSION

In summary, we successfully showed the main uptake pathways of the cationic, neutral and anionic liposomes in U87MG and NIH/3T3 cells, respectively using LSCM live cell imaging. This study provides a better understanding on the cellular uptake mechanisms of the liposomes, which could contribute significantly to development of liposome-based drug delivery systems.

## ACKNOWLEDGMENTS AND DISCLOSURES

This research was supported by the Basic Science Research Program (NRF2014R1A1A2053373) and the Pioneer Research Center Program (NRF2014M3C1A3054153) of

the National Research Foundation of Korea, funded by the Ministry of Education, Science and Technology.

## REFERENCES

- Kim J-S. Liposomal drug delivery system. *J Pharm Investig.* 1-6.
- Bozzuto G, Molinari A. Liposomes as nanomedical devices. *Int J Nanomedicine.* 2015;10:975.
- Çağdaş M, Sezer AD, Bucak S. Liposomes as potential drug carrier systems for drug Delivery. INTECH; 2014.
- Miller CR, Bondurant B, McLean SD, McGovern KA, O'Brien DF. Liposome-cell interactions in vitro: effect of liposome surface charge on the binding and endocytosis of conventional and sterically stabilized liposomes. *Biochemistry.* 1998;37(37):12875–83.
- Bareford LM, Swaan PW. Endocytic mechanisms for targeted drug delivery. *Adv Drug Deliv Rev.* 2007;59(8):748–58.
- Kou L, Sun J, Zhai Y, He Z. The endocytosis and intracellular fate of nanomedicines: implication for rational design. *Asian J Pharm Sci.* 2013;8(1):1–10.
- El-Sayed A, Harashima H. Endocytosis of gene delivery vectors: from clathrin-dependent to lipid raft-mediated endocytosis. *Mol Ther.* 2013;21(6):1118–30.
- Fröhlich E. The role of surface charge in cellular uptake and cytotoxicity of medical nanoparticles. *Int J Nanomedicine.* 2012;7(1):5577–91.
- Khodjakov A, Rieder CL. Imaging the division process in living tissue culture cells. *Methods.* 2006;38(1):2–16.
- Huang Y, Fenech M, Shi Q. Micronucleus formation detected by live-cell imaging. *Mutagenesis.* 2011;26(1):133–8.
- Watson P. Live cell imaging for target and drug discovery. *Drug News Perspect.* 2009;22(2):69–79.
- Hornick JE, Bader JR, Tribble EK, Trimble K, Breunig JS, Halpin ES, *et al.* Live-cell analysis of mitotic spindle formation in taxol-treated cells. *Cell Motil Cytoskeleton.* 2008;65(8):595–613.
- Fiume G, Di Rienzo C, Marchetti L, Pozzi D, Caracciolo G, Cardarelli F. Single-cell real-time imaging of transgene expression upon lipofection. *Biochem Biophys Res Commun.* 2016;474(1):8–14.
- Tian T, Wang Y, Wang H, Zhu Z, Xiao Z. Visualizing of the cellular uptake and intracellular trafficking of exosomes by live-cell microscopy. *J Cell Biochem.* 2010;111(2):488–96.
- Hartwell LH, Kastan MB. Cell cycle control and cancer. *Science.* 1994;266(5192):1821–8.
- Vaupel P, Kallinowski F, Okunieff P. Blood flow, oxygen and nutrient supply, and metabolic microenvironment of human tumors: a review. *Cancer Res.* 1989;49(23):6449–65.
- Cone Jr CD. The role of the surface electrical transmembrane potential in normal and malignant mitogenesis. *Ann N Y Acad Sci.* 1974;238:420–35.
- Kang JH, Battogtokh G, Ko YT. Folate-targeted liposome encapsulating chitosan/oligonucleotide polyplexes for tumor targeting. *AAPS PharmSciTech.* 2014;15(5):1087–92.

19. Ko YT, Falcao C, Torchilin VP. Cationic liposomes loaded with proapoptotic peptide D-(KLAKLAK)<sub>2</sub> and Bcl-2 antisense oligodeoxynucleotide G3139 for enhanced anticancer therapy. *Mol Pharm*. 2009;6(3):971–7.
20. Ruttala HB, Ko YT. Liposome encapsulated albumin-paclitaxel nanoparticle for enhanced antitumor efficacy. *Pharm Res*. 2015;32(3):1002–16.
21. Vranic S, Boggetto N, Contremoulins V, Mornet S, Reinhardt N, Marano F, *et al*. Deciphering the mechanisms of cellular uptake of engineered nanoparticles by accurate evaluation of internalization using imaging flow cytometry. *Part Fibre Toxicol*. 2013;10(2):45.
22. Patel H, Marley S, Greener L, Gordon M. Subcellular distribution of p210BCR-ABL in CML cell lines and primary CD34<sup>+</sup> CML cells. *Leukemia*. 2008;22(3):559–71.
23. Mufamadi MS, Pillay V, Choonara YE, Du Toit LC, Modi G, Naidoo D, *et al*. A review on composite liposomal technologies for specialized drug delivery. *J Drug Deliv*. 2011;2011:939851.
24. Kang JH, Ko YT. Lipid-coated gold nanocomposites for enhanced cancer therapy. *Int J Nanomedicine*. 2015;10(Spec Iss):33–45.
25. Ruttala HB, Ko YT. Liposomal co-delivery of curcumin and albumin/paclitaxel nanoparticle for enhanced synergistic antitumor efficacy. *Colloids Surf B: Biointerfaces*. 2015;128:419–26.
26. Allen TM, Cullis PR. Liposomal drug delivery systems: from concept to clinical applications. *Adv Drug Deliv Rev*. 2013;65(1):36–48.
27. Torchilin VP. Recent advances with liposomes as pharmaceutical carriers. *Nat Rev Drug Discov*. 2005;4(2):145–60.
28. Immordino ML, Dosio F, Cattel L. Stealth liposomes: review of the basic science, rationale, and clinical applications, existing and potential. *Int J Nanomedicine*. 2006;1(3):297.
29. Elouahabi A, Ruyschaert J-M. Formation and intracellular trafficking of lipoplexes and polyplexes. *Mol Ther*. 2005;11(3):336–47.
30. Honary S, Zahir F. Effect of zeta potential on the properties of nano-drug delivery systems—a review (Part 1). *Trop J Pharm Res*. 2013;12(2):255–64.
31. Adami RC, Seth S, Harvie P, Johns R, Farn R, Fosnaugh K, *et al*. An amino acid-based amphoteric liposomal delivery system for systemic administration of siRNA. *Mol Ther*. 2011;19(6):1141–51.
32. Tannock IF, Rotin D. Acid pH in tumors and its potential for therapeutic exploitation. *Cancer Res*. 1989;49(16):4373–84.
33. Estrella V, Chen T, Lloyd M, Wojtkowiak J, Cornnell HH, Ibrahim-Hashim A, *et al*. Acidity generated by the tumor microenvironment drives local invasion. *Cancer Res*. 2013;73(5):1524–35.
34. Li Y-L, Van Cuong N, Hsieh M-F. Endocytosis pathways of the folate tethered star-shaped PEG-PCL micelles in cancer cell lines. *Polymers*. 2014;6(3):634–50.
35. dos Santos T, Varela J, Lynch I, Salvati A, Dawson KA. Effects of transport inhibitors on the cellular uptake of carboxylated polystyrene nanoparticles in different cell lines. *PLoS One*. 2011;6(9):e24438.
36. Ivanov AI. Pharmacological inhibition of endocytic pathways: is it specific enough to be useful? *Exocytosis and Endocytosis*. 2008:15–33.
37. Stan RV. Endocytosis pathways in endothelium: how many? *Am J Phys Lung Cell Mol Phys*. 2006;290(5):L806–L8.
38. Dutta D, Donaldson JG. Search for inhibitors of endocytosis: intended specificity and unintended consequences. *Cell Logist*. 2012;2(4):203–8.
39. Falcone S, Cocucci E, Podini P, Kirchhausen T, Clementi E, Meldolesi J. Macropinocytosis: regulated coordination of endocytic and exocytic membrane traffic events. *J Cell Sci*. 2006;119(22):4758–69.
40. Parton RG, Simons K. The multiple faces of caveolae. *Nat Rev Mol Cell Biol*. 2007;8(3):185–94.
41. Lajoie P, Nabi IR. Lipid rafts, caveolae, and their endocytosis. *Int Rev Cell Mol Biol*. 2010;282:135–63.
42. Khalil IA, Kogure K, Akita H, Harashima H. Uptake pathways and subsequent intracellular trafficking in nonviral gene delivery. *Pharmacol Rev*. 2006;58(1):32–45.
43. Brodsky FM, Chen C-Y, Knuehl C, Towler MC, Wakeham DE. Biological basket weaving: formation and function of clathrin-coated vesicles. *Annu Rev Cell Dev Biol*. 2001;17(1):517–68.